ACS APPLIED MATERIALS & INTERFACES

Research Article

www.acsami.org

N-Doped Graphene–VO_2(B) Nanosheet-Built 3D Flower Hybrid for Lithium Ion Battery

C. Nethravathi,*[,†] Catherine R. Rajamathi,[‡] Michael Rajamathi,*[,‡] Ujjal K. Gautam,[§] Xi Wang,*[,†] Dmitri Golberg,[†] and Yoshio Bando[†]

[†]International Center for Materials, Nanoarchitectonics (MANA), National Institute for Materials Science (NIMS), Namiki 1-1, Tsukuba, Ibaraki 305-0044, Japan

[‡]Materials Research Group, Department of Chemistry, St. Joseph's College, 36 Lalbagh Road, Bangalore 560 027, India

[§]New Chemistry Unit, Jawaharlal Nehru Centre for Advanced Scientific Research, Bangalore 560 064, India

Supporting Information

ABSTRACT: Recently, we have shown that the graphene–VO_2(B) nanotube hybrid is a promising lithium ion battery cathode material (Nethravathi et al. *Carbon*, **2012**, *50*, 4839–4846). Though the observed capacity of this material was quite satisfactory, the rate capability was not. To improve the rate capability we wanted to prepare a graphene–VO_2(B) hybrid in which the VO_2(B) would be built on 2D nanosheets that would enable better electrode–electrolyte contact. Such a material, a N-doped graphene–VO_2(B) nanosheet-built 3D flower hybrid, is fabricated by a single-step hydrothermal reaction within a mixture of ammonium vanadate and colloidal dispersion of graphite oxide. The 3D VO_2(B) flowers which are uniformly distributed on N-doped graphene are composed of ultrathin 2D nanosheets. When used in lithium ion batteries, this material exhibits a large capacity, high rate capability, and excellent cycling stability. The enhanced performance results from its unique features: excellent electronic conductivity associated with the N-doped graphene, short transportation length for lithium ions related to ultrathin nanosheets, and improved charge transfer due to the anchoring of the VO_2(B) flowers to N-doped graphene.

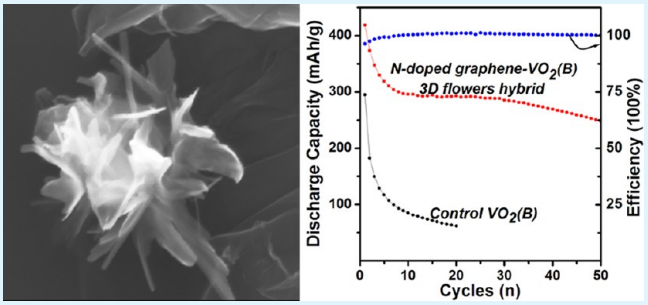

KEYWORDS: *N-doped graphene, VO_2(B), nanoflowers, lithium ion battery*

1. INTRODUCTION

VO_2(B), a metastable monoclinic phase of vanadium oxide, has been studied as a potential electrode material for aqueous and nonaqueous rechargeable lithium ion batteries (LIBs).[1−7] As a cathode material, VO_2(B) delivers a maximum reversible capacity of 320 $mAhg^{-1}$ in the range of 4–1 V in nonaqueous lithium cells,[1,3,5,8] thus higher than that of the most commonly used cathode material, $LiCoO_2$. VO_2(B) is made of distorted VO_6 octahedra which share both corners and edges and has perovskite-like cavities with four capped faces. Diffusion of lithium in VO_2(B) is parallel to the [010] crystal orientation, and lithium insertion leads to predominant uniaxial expansion of the perovskite-like cavities.[1,5] As the edge sharing of octahedra is along the direction of lattice expansion, there is an increased resistance to V–O bond cleavage during lithium intercalation. Hence, unlike the other oxides of vanadium, VO_2(B) is quite stable during lithium intercalation–deintercalation cycles, making it a good electrode material for lithium ion batteries.

Various nanostructures such as 1D nanobelts,[9] nanorods,[10] nanowires,[11] nanotubes,[5,12] and 0D nanoparticles[7,8] of VO_2(B) have been studied as cathode materials for LIBs. However there has been no such studies on 2D nanostructures or 3D nanostructures composed of 2D nanosheets of VO_2(B). The 0D and 1D structures generally exhibit low capacity (<320 $mAhg^{-1}$) and poor cycling stability. The poor performance of the material in these cases has been attributed to the formation of aggregates and collapse of structures due to the high surface energy associated with the nanostructures. Studies have shown that, in general, 3D nanomaterials, like nanoflowers or hollow spheres composed of 2D nanosheets,[13−15] exhibit enhanced capacity and stability compared to the 1D[9,16] and 0D nanostructures. These 3D structures are constituted of nanosubunits which contribute to the high surface area and stability toward huge volume variations that occur during lithiation/delithiation. Though the 3D nanostructures are better than 0D/1D structures in terms of electrochemical performance, their observed capacity is still lower than the theoretical capacity, possibly due to a poor charge transfer.

On one hand, it is still a challenge to fabricate VO_2(B) 3D structures composed of 2D nanosheets, and on the other, the electrode materials for lithium ion battery application usually

Received: January 16, 2013
Accepted: March 13, 2013
Published: March 13, 2013

   dx.doi.org/10.1021/am400202v | *ACS Appl. Mater. Interfaces* 2013, 5, 2708–2714

suffer from their low electron/ion conductivity.[17] In general, hybridization of the electroactive nanomaterial with graphene has been shown to improve the performance of the electrodes in terms of stability and capacity delivered. The lightweight graphene assists in charge transfer due to its high conductivity. The synergy of the electrical/mechanical properties and high surface area of graphene with the nanoparticle properties is expected to enhance the overall performance of the hydrids.[17]

Recently we reported the enhanced electrochemical performance of a graphene—VO_2(B) nanotube hybrid.[18] Though the observed capacity of this material was quite satisfactory the rate capability was not. Even at a moderately high charging rate the capacity dropped down substantially. Poor charge transfer at the electrode material−electrolyte interface could be the reason for the low rate capability. Keeping this in mind, we wanted to prepare a graphene−VO_2(B) hybrid in which the VO_2(B) nanostructure is built on 2D nanosheets which would enable better electrode−electrolyte contact. We could achieve this goal through a simple modification to our earlier synthesis procedure. Here we present a one-step preparation of N-doped graphene−VO_2(B) 5−10 nm thick petal-like nanosheet-built 3D flower hybrids. Hydrothermal reduction of ammonium vanadate in the presence of colloidal dispersion of graphite oxide (GO) results in simultaneous reduction of GO to graphene and formation of VO_2(B).[18] The ammonium ions present in the reaction mixture act as a source of nitrogen, thus resulting in the formation of N-doped graphene. Formic acid has been used in the reaction to create the necessary acidity and reductive atmosphere for the formation of VO_2(B).[19] The VO_2(B) flowers are constructed from ultrathin nanosheets. Therefore, the interfacial kinetics and intercalation properties of the Li ion are significantly improved due to their synergetic superiorities with adequate electrode−electrolyte contact. When used in LIBs, this material exhibits a large capacity, high rate capability, and excellent cycling stability owing to its unique features.

2. EXPERIMENTAL SECTION

2.1. Synthesis of GO. The method of Hummers and Offeman[20] was adopted to prepare GO from graphite powder. About 1 g of graphite powder was added to 23 mL of cooled (to 0 °C) concentrated H_2SO_4. About 3 g of $KMnO_4$ was added gradually under stirring and cooling, so that the temperature of the mixture was maintained below 20 °C. The mixture was then stirred at 35 °C for 30 min. About 46 mL of distilled water was slowly added to increase the temperature to 98 °C, and the mixture was maintained at that temperature for 15 min. The reaction was terminated by adding 140 mL of distilled water followed by the addition of 10 mL of 30% H_2O_2 solution. The solid product was separated by centrifugation, washed repeatedly with 5% HCl solution until sulfate could not be detected with $BaCl_2$, then washed 3−4 times with acetone, and dried in an air oven at 65 °C overnight.

2.2. Synthesis of N-Doped Graphene−VO_2(B) Nanosheet-Built 3D Flower Hybrid. The N-doped graphene−VO_2(B) nanosheet-built 3D flower hybrid was synthesized by a slight modification of the procedure employed for the synthesis of the graphene−VO_2(B) nanotube hybrid.[18] To facilitate the 2D nanostructure formation, we doubled the GO content. A mixture containing 120 mg of ammonium vanadate and 300 mg of GO was dissolved in 20 mL of water by sonication for 30 min. To the GO−vanadate solution, 20 mL of 0.1 M formic acid was added drop by drop under constant stirring. At the end of the addition, the pH was 2.5. The mixture was transferred into a Teflon-lined stainless steel autoclave and sealed. The autoclave was heated at 180 °C for 72 h. At the end of 72 h the autoclave was cooled to room temperature, and the dark green solid obtained was separated by centrifugation, washed with copious amounts of water followed by acetone, and dried at 65 °C for 30 min. For comparison, N-doped graphene and pure VO_2(B) were synthesized by similar procedures. N-doped graphene was synthesized as explained above except that an equivalent amount of ammonia was used instead of ammonium vanadate. Pure VO_2(B) was synthesized as explained above without adding GO and using 240 mg of ammonium vanadate.

2.3. Electrochemical Studies. The electrochemical properties of N-doped graphene−VO_2(B) nanosheet-built 3D flower hybrids and a control VO_2(B) nanostructure were measured using a three-electrode cell. The working electrode was prepared by pressing the slurry of 80% N-doped graphene−VO_2(B) nanosheet-built 3D flower hybrid/control VO_2(B), 10% acetylene black, and 10% polyvinylidenedifluoride (PVDF) binder (by weight) onto the copper current collector. Li metal foils were used as the reference and counter electrodes. The electrolyte was 1 M $LiClO_4$ in an ethyl carbonate (EC)−diethyl carbonate (DEC) mixture (EC/DEC = 1:1 v/v). The cells were assembled in a glovebox filled with pure argon gas. Galvanostatic discharge/charge measurements were performed over a potential range of 4−1.5 V vs Li^+/Li. The observed capacities were normalized to VO_2(B) content. Reproducibility of the electrochemical data was confirmed by repeating the experiments with at least another electrode of the same sample.

2.4. Characterization. All the samples were characterized by powder X-ray diffraction (XRD) using a Philips X'pert Pro diffractometer (Cu Kα radiation, secondary graphite monochromator, 2° 2θ per min), infrared (IR) spectroscopy using a Nicolet IR200 FTIR spectrometer (KBr pellets, 4 cm^{-1} resolution), and thermogravimetry (ThermoPlus TG 8120; 1 °C per min until 550 °C and isothermal at 550 °C for 1 h in air). Transmission electron microscopy (TEM) images were recorded with a JEOL F3000 microscope operated at 300 kV. Scanning electron microscopy (SEM) images were recorded on a Hitachi S4800 electron microscope operating at 15 kV. X-ray photoelectron spectroscopy (XPS) measurements were carried out with an ESCALab220i-XL spectrometer using a twin-anode Al Kα (1486.6 eV) X-ray source. All spectra were calibrated to the binding energy of the C 1s peak at 284.51 eV. The base pressure was around 3 × 10^{-7} Pa. Raman spectra were recorded on a Horiba Jobin-Yvon T6400 Raman spectrometer.

3. RESULTS AND DISCUSSION

The hydrothermal reaction of a mixture of colloidal dispersion of excess graphite oxide and ammonium vanadate in the presence of formic acid results in the formation of the desired hybrid. Our attempts to prepare a graphene−VO_2(B) nanosheet-built 3D structure keeping the GO:ammonium vanadate ratio the same as in our earlier work[18] and altering the reaction conditions such as temperature, duration, and pH failed. Only when the GO content was doubled could we obtain the desired composite. Vanadate ion and GO undergo simultaneous reduction to VO_2(B) and graphene, respectively, leading to the hybrid. Thermogravimetric analysis (Supporting Information, Figure S1) of the hybrid carried out in air suggests that 31% of the mass of the hybrid is due to VO_2(B).

In the XRD pattern of the N-doped graphene−VO_2(B) nanosheet-built 3D flower hybrid (Figure 1a), the reflections due to both VO_2(B) and graphene could be observed. All the Bragg reflections, other than the broad 002 and 100 reflections due to graphite, could be indexed to monoclinic VO_2(B) [JCPDS 81-2392]. No peaks related to impurities were observed. The very broad reflections due to 002 and 100 planes of graphite suggest the presence of largely exfoliated graphene layers. The reflections of VO_2(B) are also quite broad owing to small crystallite sizes. The reflections in the XRD pattern of the control VO_2(B) (Figure 1b) match well with the reflections, other than the ones due to graphene, found in the pattern of the hybrid. The broad 002 and 100 reflections of

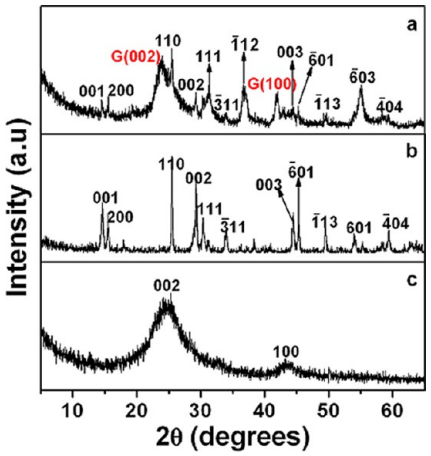

Figure 1. XRD patterns of (a) N-doped graphene–VO_2(B) nanosheet-built 3D flower hybrid, (b) control VO_2(B) prepared under similar conditions, and (c) graphene obtained by hydrothermal treatment of GO in the presence of ammonia.

graphite in the XRD pattern of the solid obtained when GO was subjected to the hydrothermal reaction in the absence of ammonium vanadate confirm that GO gets reduced to graphene during the formation of the hybrid.

In the IR spectrum of GO (Supporting Information, Figure S2a), the O–H stretching vibration at 3400 cm^{-1}, C═O stretching of COOH at 1726 cm^{-1}, O–H bending vibrations, and the skeletal ring vibrations at ∼1622 cm^{-1} and an absorption due to tertiary C–OH groups at 1393 cm^{-1} confirm the presence of various oxygen-containing functional groups in GO.[21] In contrast, in the IR spectrum of the hybrid (Supporting Information, Figure S2b) the peaks due to GO have disappeared, indicating GO reduction. There is a weak peak corresponding to C═O stretching vibration of COOH at 1726 cm^{-1} suggesting that the reduction is incomplete. The bands at 1007 and 539 cm^{-1} due to (V═O) and (V–O–V) vibrations, respectively, are due to the VO_2 component of the hybrid.[8]

In the low-magnification SEM image of the hybrid (Figure 2a) we observe uniform distribution of 3D flowers of VO_2(B) on graphene. The uniform distribution is also confirmed from the energy-dispersive spectroscopy (EDS) recorded from various regions of the sample. The high-magnification SEM image (Figure 2b) shows that each 3D flower anchored on graphene is a cluster of thin platelets. The flower consists of petal-like layers with a thickness of 5–10 nm (Figure 2b).

The bright-field TEM images (Figure 2c and d) reveal the formation of the flowers on thin corrugated graphene sheets. The selected area electron diffraction pattern (SAED) (Figure 2d inset) recorded from a region of transparent layers of graphene shows diffuse rings that could be indexed to 002 and 100 reflections of graphite. The flowers are 500 nm–1 μm in diameter. The morphology of VO_2(B) is controlled by the pH of the reaction medium. In this study the synthesis of the hybrid was carried out in excess of GO compared to the previous report where VO_2(B) nanotubes were formed in the presence of GO.[18] The difference in morphology of VO_2(B), when the GO content is changed, could possibly be due to the fact that the pH of the reaction medium is lowered as the amount of acidic GO increases. While the lower pH does not affect the formation of the VO_2(B) phase, it changes its morphology.[19] The oxygen-bearing functional groups on GO

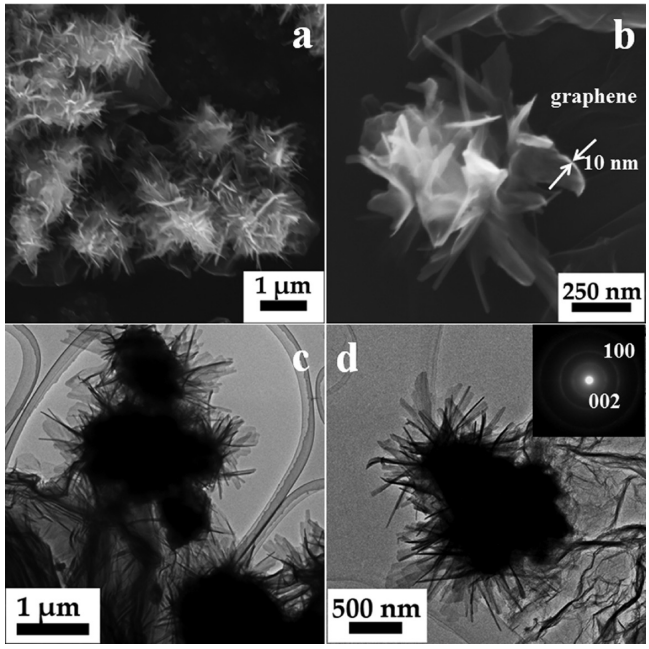

Figure 2. (a) Low- and (b) high-magnification SEM images and bright-field TEM images (c) and (d) of N-doped graphene–VO_2(B) nanosheet-built 3D flower hybrid. The selected area electron diffraction pattern from a region of transparent layers of graphene is given in the inset in (d).

could possibly act as nucleating centers for the formation of the flowers.[22,23]

The G band (∼1581 cm^{-1}) associated with the scattering of sp^2 carbon domains and disorder-related D band (∼1345 cm^{-1}) in the Raman spectrum of the N-doped graphene–VO_2(B) nanosheet-built 3D flower hybrid (Figure 3a) are characteristic

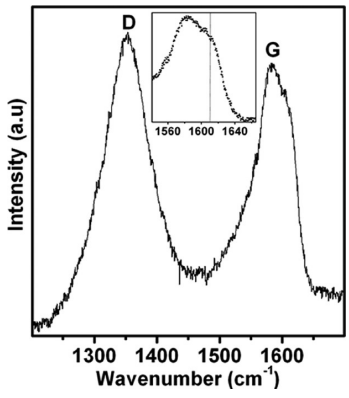

Figure 3. Raman spectrum of graphene in N-doped graphene–VO_2(B) nanosheet-built 3D flower hybrid.

of graphene.[24,25] The inset shows the splitting of the G band due to nitrogen doping, as reported in the literature.[26] It is indeed surprising since this splitting was not observed in the graphene–VO_2(B) nanotube hybrid that was prepared by a similar method.[18] Ammonium ions present in the reaction mixture have acted as the source for the dopant in the present reaction.[27] The electron energy loss spectrum of the hybrid (Supporting Information Figure S3) exhibits a peak at 285 eV due to the 1s–π^* transition and another between 290 and 315 eV that correspond to the 1s–σ^* transitions confirming the presence of graphene in the hybrid.[28,29]

A detailed chemical analysis of the hybrid was carried out using high-angle annular dark-field (HAADF) scanning transmission electron microscopy (STEM) and EDS elemental mapping. Figure 4a presents a HAADF STEM image of the

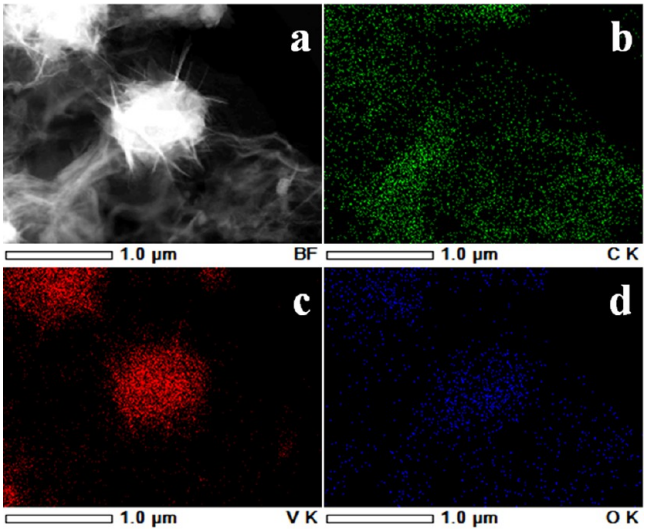

Figure 4. HAADF STEM image (a) and the spatially resolved C (b), V (c), and O (d) elemental maps of a N-doped graphene–VO_2(B) nanosheet-built 3D flower hybrid.

hybrid. The elemental maps of the constituting elements C, V, and O (Figure 4b–d) clearly demonstrate a well-defined compositional profile of the VO_2(B) flowers on graphene.

In the core level XPS spectrum of GO (Figure 5a), in addition to the main peak due to sp^2 carbon atoms, there are three other peaks that are associated with the functional groups

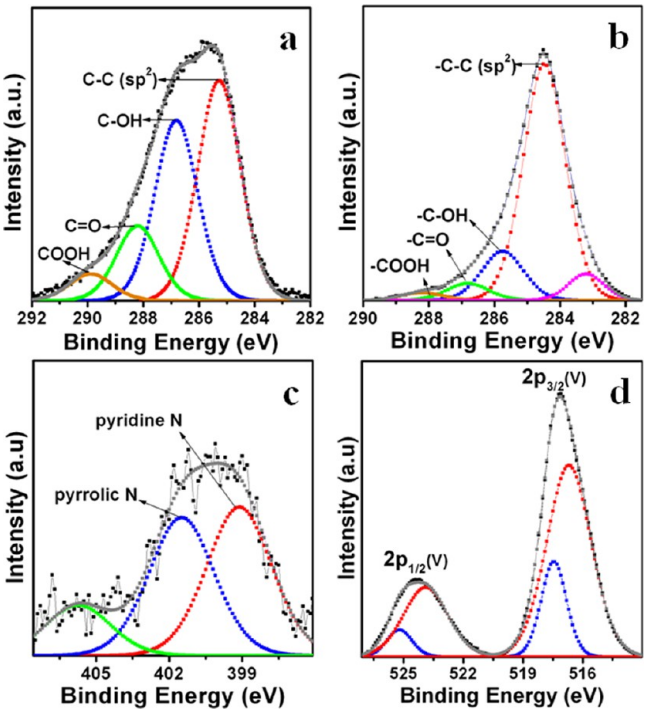

Figure 5. Core-level C 1s XPS spectrum of GO (a), C 1s (b), N 1s (c), and V 2p (d) XPS spectra of the N-doped graphene–VO_2(B) nanosheet-built 3D flower hybrid.

on GO. The intensities of these additional peaks are considerably reduced in the case of the hybrid (Figure 5b), suggesting reduction of GO to graphene in the hybrid. The N-doping of graphene indicated by the Raman spectrum (Figure 3) was further confirmed by XPS. The N 1s XPS spectrum of the hybrid (Figure 5c) indicates the presence of pyrrolic (401.49 eV) and pyridinic (399.10 eV) nitrogen species, as commonly observed for N-doped carbon materials.[26] The binding energy in the case of V 2p peaks (Figure 5d) is slightly shifted to higher values compared to those reported for VO_2(B). While the expected binding energies are 516.3 and 524.1 eV, the observed values are 516.87 and 524.47 eV. Similarly, a shift to lower binding energy (from 532.42 and 534.18 eV to 531.88 and 533.36 eV) has been observed in the case of the functional groups on graphene in the hybrid. These observations suggest that VO_2(B) flowers are anchored to N-doped graphene through weak chemical interactions.

To understand the mechanism of formation of VO_2(B) flowers on graphene, we recovered the reaction mixture at different stages of the reaction. The bright-field TEM images of the intermediates obtained at various time intervals are shown in Figure 6. Nucleation of VO_2(B) on graphene starts within 12

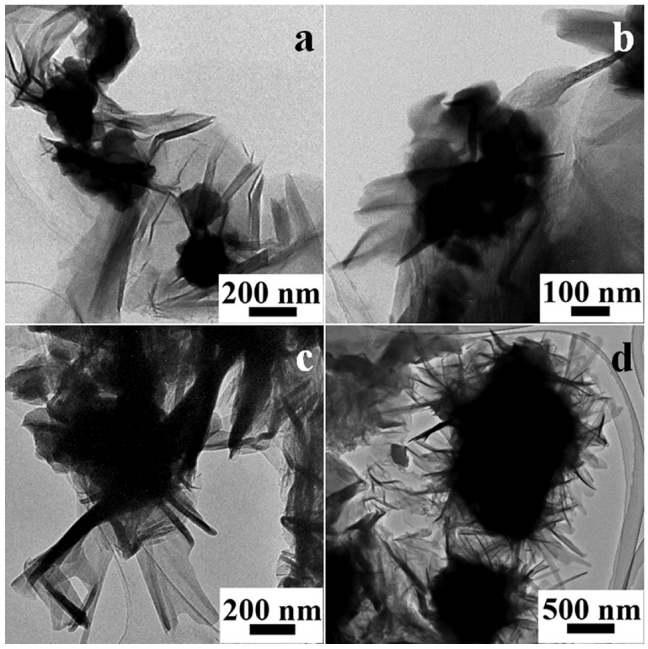

Figure 6. Bright-field TEM images of the intermediates obtained at 12 (a), 24 (b), and 48 (c) h compared with that of the hybrid obtained after 72 h (d).

h. Initially the VO_x species nucleate as irregular sheets on graphene, which eventually branch out into flowers after 48 h and grow into full-fledged flowers in 72 h.

The motivation to synthesize this hybrid was our belief that the unique hybrid structure may endow the material with superior electrochemical performance better than what was observed for the graphene–VO_2(B) nanotube hybrid.[18] To verify this hypothesis, the electrochemical performance of the hybrid was evaluated for Li insertion/extraction in comparison to that of the control VO_2(B) nanoparticles using lithium half-cells.

Figure 7a shows the cycling performances of the hybrid and pure VO_2(B) nanoparticles at a current density of 50 $mAhg^{-1}$.

dx.doi.org/10.1021/am400202v | ACS Appl. Mater. Interfaces 2013, 5, 2708–2714

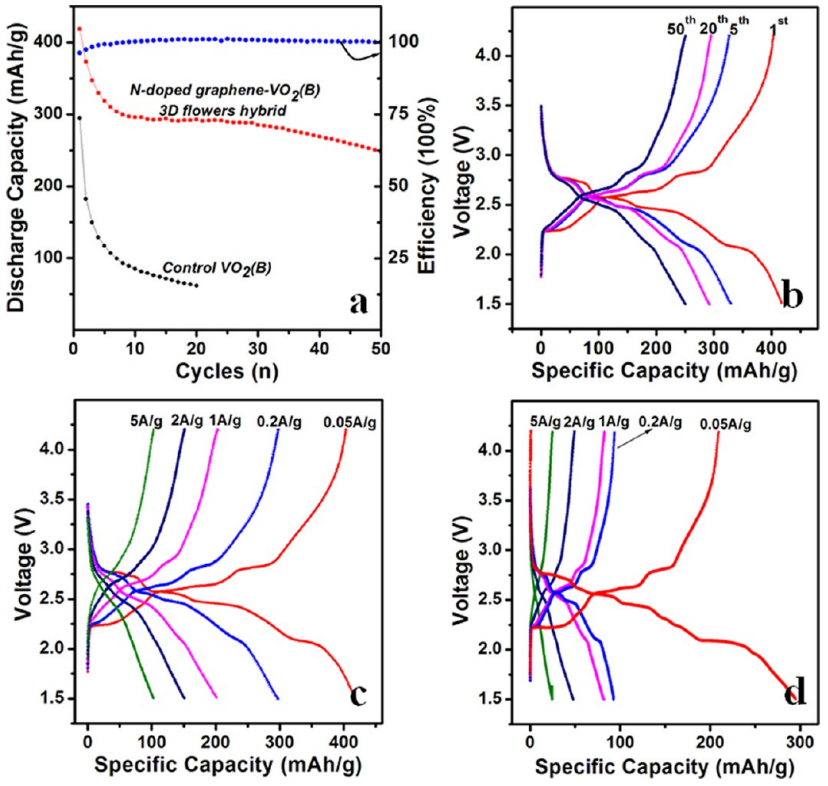

Figure 7. Cycling performance of N-doped graphene–VO_2(B) nanosheet-built 3D flower hybrid and a control VO_2(B) at a current density of 50 $mAhg^{-1}$ (a). The capacities are based on the mass of VO_2(B) in the hybrid (mass of VO_2(B) was estimated to be 31%). The charge–discharge curves of N-doped graphene–VO_2(B) nanosheet-built 3D flower hybrid, as the cell is repeatedly charged–discharged at a current density of 50 $mAhg^{-1}$ (b). Charge/discharge curves of N-doped graphene–VO_2(B) nanosheet-built 3D flower hybrid (c) and control VO_2(B) (d) at different current densities.

It is clear that our sample exhibits much better cycling performance than the control specimen. After 50 cycles, the hybrid exhibits about 60% retention (251 $mAhg^{-1}$, see Table 1) of the initial capacity, leading to a low 0.79% capacity loss per cycle, while the control nanoparticle sample shows a fast capacity fading and only 21% retention (61.8 $mAhg^{-1}$) after only 20 cycles, leading to a 3.9% capacity loss per cycle. The enhanced electrochemical performance observed here is quite similar to what had been observed for the related graphene–V_2O_5 hybrids which show higher capacity and better cycle life compared to pure V_2O_5.[30−33]

Table 1. Summary of the Electrochemical Behavior of N-Doped Graphene–VO_2(B) Nanosheet-Built 3D Flower Hybrid and Control VO_2(B) as a Cathode Material for Nonaqueous LIB

discharge capacity ($mAhg^{-1}$)		
cycle number	N-doped graphene–VO_2(B) 3D flowers hybrid	control VO_2(B)
1	418	294
20	300	61.8
50	251	-
fading rate (%)	0.79	3.9
rate capacity		
current density (Ag^{-1})	specific capacity ($mAhg^{-1}$)	
0.05	418	295
0.2	297	92
1	199	81
2	151	47
5	102	24

In addition, the Coulombic efficiency of the hybrid reaches ~100% (Figure 7a) after the first cycle, demonstrating very good reversibility. Figure 7b shows the charge–discharge curves of the hybrid at the 1st, 5th, 20th, and 50th cycle, respectively. There is no large decrease in capacity, further indicating its structural advantage in improvement of LIB performance. It should be noted that the hybrid exhibited ultrahigh capacity of 418 $mAhg^{-1}$, larger than the theoretical capacity (320 $mAhg^{-1}$) of VO_2(B) similar to the graphene–VO_2(B) nanotube hybrid.[18] This may be due to its unique features, such as high surface area (71.59 $m^2\ g^{-1}$; see Supporting Information, Figure S5) associated with thin nanosheets constituting the flowers[8] and also the enhanced conductivity and charge transfer due to the presence of N-doped graphene.[34−36] More importantly, our hybrid showed much improved rate capabilities, as shown in Figure 7c, Table 1, and Supporting Information, Figure S6. The sample maintained high capacity of 191 and 151 $mAhg^{-1}$ when the current density was increased to 1 and 2 Ag^{-1}, respectively. Even at a larger current density of 5 Ag^{-1}, our hybrids still showed a high capacity of 102 $mAhg^{-1}$. In contrast, the control VO_2(B) (Figure 7d, Table 1) rapidly decayed from 295 $mAhg^{-1}$ at a current density of 0.05 Ag^{-1} to 92 $mAhg^{-1}$ at 1 Ag^{-1}, to 47 $mAhg^{-1}$ at 2 Ag^{-1}, and to 24 $mAhg^{-1}$ at 2 Ag^{-1}, respectively.

This feature of the N-doped graphene–VO_2(B) nanosheet-built 3D flower hybrid is an improvement over the performance of the graphene–VO_2(B) nanotube composite[18] which showed poorer rate capability (Table 2). Even at a charging rate of 100

Table 2. Comparison of Discharge Capacity of N-Doped Graphene−VO_2(B) Nanosheet-Built 3D Flower Hybrid with the Capacities Reported for Other VO_2(B) Materials

cathode material	discharge current density (Ag^{-1})	potential range (V)	capacity ($mAhg^{-1}$)	reference
N-doped graphene−VO_2(B) 3D flowers	0.05	4.0−1.5	418	present work
	0.2		297	
	1		199	
graphene−VO_2(B) tubes	0.04		450	16
	0.1		180	

$mAhg^{-1}$ the capacity of the graphene−VO_2(B) nanotube composite decreased to ∼200 $mAhg^{-1}$, while the N-doped graphene−VO_2(B) nanosheet-built 3D flower hybrid exhibited a capacity of ∼300 $mAhg^{-1}$ at a charging rate of 200 mAg^{-1}. Only at the charging rate of 1 Ag^{-1} the capacity reached ∼200 $mAhg^{-1}$. Thus, the N-doped graphene−VO_2(B) nanosheet-built 3D flower hybrid is indeed an improved and promising LIB cathode material. The 3D nanoflower hybrid shows higher capacity at high discharge rates due to improved charge transfer owing to a better contact between the active materials and graphene sheets. The observation of high capacity even when the charge−discharge current densities are very high points clearly to the effective charge transfer in the material.

The enhanced electrochemical performance is attributed to the unique architectures of the new material. First, the ultrathin VO_2(B) nanosheets (5−10 nm) not only render a very short transport length for lithium ions during insertion/extraction but also bring high surface area, giving rise to a large contact area between the active material and the electrolyte, favoring a high rate charge/discharge performance. Second, the N-doped graphene matrix induces much higher conductivity for the hybrids.[34−36] N-doping in graphene is known to significantly alter its physiochemical properties and in particular is expected to introduce additional n-type carriers in graphene which is crucial for various applications like enhanced catalysis for energy conversion/storage.[34−36] Third, the anchoring of the 3D VO_2(B) flowers to N-doped graphene not only improves the charge transfer but also prevents aggregation and loss of surface area. The TEM image (Supporting Information, Figure S7) of the spent electrode (after 50 cycles) shows that the 3D flower morphology of VO_2(B) remains largely intact. The above synergetic effects originated from N-doped graphene−VO_2(B) 3D flowers are responsible for the excellent electrochemical performance of the electrode.

4. CONCLUSIONS

A graphene−VO_2(B) hybrid in which ultrathin nanosheet-built VO_2(B) flowers are anchored on graphene sheets has been prepared. The 3D flower morphology constructed with ultrathin nanosheets has led to a high surface area and a better contact with the graphene matrix. These result in enhanced charge transfer and superior electrochemical performance. In addition, the graphene matrix prevents agglomeration of VO_2(B) flowers leading to improved cycle life.

■ ASSOCIATED CONTENT

Ⓢ Supporting Information

TG data, IR spectra, EELS, BET surface area data, O 1s core-level X-ray photoelectron spectrum of the hybrid, and TEM images of the spent electrode material. This material is available free of charge via the Internet at http://pubs.acs.org.

■ AUTHOR INFORMATION

Corresponding Author

*E-mail: nethravathic@gmail.com; mikerajamathi@rediffmail.com; wang.xi2@nims.go.jp.

Notes

The authors declare no competing financial interest.

■ ACKNOWLEDGMENTS

This work was supported by the International Center for Materials Nanoarchitectonics (MANA) tenable at the National Institute for Materials Science (NIMS) and the Japan Society for Promotion of Science (JSPS). CRR and MR acknowledge the partial funding of this work by DST, India. The authors thank Drs. Yamada, M. Mitome, and N. Kawamoto of MANA-NIMS for technical support.

■ REFERENCES

(1) Murphy, D. W.; Christian, P. A. *Science* **1979**, *205*, 651−656.
(2) Li, W.; Dahn, J. R.; Wainwright, D. S. *Science* **1994**, *264*, 1115−1118.
(3) James, G. *Science* **1994**, *264*, 1084.
(4) Guo, Y. G.; Hu, J. S.; Wan, L. J. *Adv. Mater.* **2008**, *20*, 2878−2887.
(5) Chernova, N. A.; Roppolo, A. C.; Dillonb, M.; Whittingham, M. *J. Mater. Chem.* **2009**, *19*, 2526−2552.
(6) Li, W.; Dahn, J. R. *J. Electrochem. Soc.* **1995**, *142*, 1742−1746.
(7) Tang, C. S.; Manthiram, A. *J. Electrochem. Soc.* **1997**, *144*, 520−524.
(8) Baudrin, E.; Sudant, G.; Larcher, D.; Dunn, B.; Tarascon, J. M. *Chem. Mater.* **2006**, *18*, 4369−4374.
(9) Zhao, Q.; Jiao, L.; Peng, W.; Gao, H.; Yang, Y.; Wang, Q.; Du, H.; Li, L.; Qi, Z.; Si, Y.; Wang, Y.; Yuan, H. *J. Power Sources* **2012**, *199*, 350−354.
(10) Chen, Z.; Gao, S.; Jianga, L.; Wei, M.; Wei, K. *Mater. Chem. Phys.* **2010**, *121*, 254−258.
(11) Armstrong, G.; Canales, J.; Armstrong, A. R.; Bruce, P. G. *J. Power Sources* **2008**, *178*, 723−728.
(12) Patzke, G. R.; Krumeich, F.; Nesper, R. *Angew. Chem., Int. Ed.* **2002**, *41*, 2446−2461.
(13) Liu, H. M.; Wang, Y. G.; Wang, K. X.; Hosono, E.; Zhou, H. S. *J. Mater. Chem.* **2009**, *19*, 2835−2840.
(14) Zhang, S. D.; Li, Y. M.; Wu, C. Z.; Zheng, F.; Xie, Y. *J. Phys. Chem. C* **2009**, *113*, 15058−15067.
(15) Fang, X.; Ye, C.; Zhang, L.; Zhang, J.; Zhao, J.; Yan, P. *Small* **2005**, *4*, 422−428.
(16) Fang, X.; Wu, L.; Hu, F. *Adv. Mater.* **2011**, *23*, 585−598.
(17) Liang, M.; Zhi, L. *J. Mater. Chem.* **2009**, *19*, 5871−5878.
(18) Nethravathi, C.; Viswanath, B.; Michael, J.; Rajamathi, M. *Carbon* **2012**, *50*, 4839−4846.
(19) Liu, J.; Li, Q.; Wang, T.; Yu, D.; Li, Y. *Angew. Chem., Int. Ed.* **2004**, *43*, 5048−5052.
(20) Hummers, W. S.; Offeman, R. E. *J. Am. Chem. Soc.* **1958**, *80*, 1339.
(21) Szabo, T.; Berkesi, O.; Forgo, P.; Josepovits, K.; Sanakis, Y.; Petridis, D.; Dekany, I. *Chem. Mater.* **2006**, *18*, 2740−2749.
(22) Wang, H.; Robinson, J. T.; Diankov, G.; Dai, H. *J. Am. Chem. Soc.* **2010**, *132*, 3270−3271.
(23) Nethravathi, C.; Anumol, E. A.; Rajamathi, M.; Ravishankar, N. *Nanoscale* **2011**, *3*, 569−571.
(24) Malard, L. M.; Pimenta, M. A.; Dresselhaus, G.; Dresselhaus, M. S. *Phys. Rep.* **2009**, *473*, 51−87.
(25) Ferrari, A. C.; Meyer, J. C.; Scardaci, V.; Casiraghi, C.; Lazzeri, M.; Mauri, F.; Piscanec, S.; Jiang, D.; Novoselov, K. S.; Roth, S.; Geim, A. K. *Phys. Rev. Lett.* **2006**, *97*, 187401.

(26) Deng, D.; Pan, X.; Yu, L.; Cui, Y.; Jiang, Y.; Qi, J.; Li, W.-X.; Fu, Q.; Ma, X.; Xue, Q.; Sun, G.; Bao, X. *Chem. Mater.* **2011**, *23*, 1188−1193.
(27) Long, D.; Li, W.; Ling, L.; Miyawaki, J.; Mochida, I.; Yoon, S-Ho. *Langmuir* **2010**, *26*, 16096−16102.
(28) Suenaga, K.; Sandre, E.; Colliex, C.; Pickard, C. J.; Kataura, H.; Iijima, S. *Phys. Rev. B* **2001**, *63*, 165408−165412.
(29) Alexandrou, I.; Scheibe, H.-J.; Kiely, C. J.; Papworth, A. J.; Amaratunga, G. A. J.; Schultrich, B. *Phys. Rev. B* **1999**, *60*, 10903−10907.
(30) Zhao, H.; Pan, L.; Xing, S.; Luo, J.; Xu, J. *J. Power Sources* **2013**, *222*, 21−31.
(31) Zhang, W.; Zeng, Y.; Xiao, N.; Hng, H. H.; Yan, Q. *J. Mater. Chem.* **2012**, *22*, 8455−8461.
(32) Rui, X.; Zhu, J.; Sim, D.; Xu, C.; Zeng, Y.; Hng, H. H.; Lim, T. M.; Yan, Q. J. *Nanoscale* **2011**, *3*, 4752−4758.
(33) Du, G.; Seng, K. H.; Guo, Z.; Liu, J.; Li, W.; Jia, D.; Cook, C.; Liu, Z.; Liu, H. *RSC Adv.* **2011**, *1*, 690−697.
(34) Wang, X.; Cao, X.; Bourgeois, L.; Guan, H.; Chen, S.; Zhong, Y.; Tang, D.-M.; Li, H.; Zhai, T.; Li, L.; Bando, Y.; Golberg, D. *Adv. Funct. Mater.* **2012**, *22*, 2682−2690.
(35) Wang, H.; Maiyalagan, T.; Wang, X. *ACS Catal.* **2012**, *2*, 781−794.
(36) Reddy, A. L. M.; Srivastava, A.; Gowda, S. R.; Gullapalli, H.; Dubey, M.; Ajayan, P. M. *ACS Nano* **2010**, *4*, 6337−6342.